

Research

Shear strength of soil by using rice husk ash waste for sustainable ground improvement

Abdelmageed Atef Abdelmageed Shehata¹ · Alex Otieno Owino¹ · Md. Yachin Islam¹ · Zakaria Hossain¹

Received: 21 September 2023 / Accepted: 26 March 2024

Published online: 10 April 2024

© The Author(s) 2024 [OPEN](#)

Abstract

In the global construction industry, areas characterized by weak and expansive soils are on the rise, necessitating effective solutions for strength enhancement. Addressing this concern, sustainable soil amendments have gained attention, with rice husk ash (RHA) from rice milling industries being a notable focus. Our experimental study aimed to assess the shear strength of this innovative construction material, introducing a unique approach that considers subgrade layers with minimal cement dosage, including upper, bottom, and double layers a novel contribution yet unexplored in existing literature. In addition to conventional mechanical testing, we employed SEM (Scanning Electron Microscopy) and EDS (Energy-Dispersive X-ray Spectroscopy) analyses to comprehensively explore the treated soils' microstructural and elemental composition aspects. Examining sixteen specimen combinations of weak expansive soil-RHA-cement, varying proportions of RHA (2%, 4%, 6%) and cement (2%, 4%, 6%) were mixed to understand their effects on shear strength parameters. Our findings revealed significant shear strength improvement in each subgrade layer, with specimen 6%RHA6%C in the lower subgrade layer exhibiting the highest cohesive strength at 143 kN/m². Notably, the double layer configuration, specimen 2%RHA6%C, achieved maximum deviatoric stresses of 383 kN/m². This novel construction material contributes to effective waste management and presents an innovative engineering solution for sustainable ground improvement, offering promising prospects for future geotechnical advancements.

Keywords Rice husk ash · Shear strength · Sustainable ground improvement · Subgrade

1 Introduction

Ground improvement is a crucial aspect of geotechnical engineering, particularly when the soil at a selected site lacks the desired mechanical properties such as cohesion, internal angle of friction, and bearing capacity [1]. Poorly compacted soil can lead to catastrophic consequences, including slope failures [2], foundation sinkage [3], and even the complete collapse of structures like tunnels, mine dumps, and buildings [3]. Several methods are used to improve ground conditions for safe and reliable construction [4]. Based on the treatment method, the engineering techniques of ground improvement can be broadly grouped into mechanical [4] and chemical stabilization [3]. Among these, mechanical stabilization is the most common and oldest technique of ground improvement [5], where the soil's density is increased by applying mechanical force and compacting the surface layers by static and dynamic loading [6]. Mechanical methods are more complex and expensive [5, 6] than chemical processes [7].

✉ Abdelmageed Atef Abdelmageed Shehata, 522d2s1@m.mie-u.ac.jp; Alex Otieno Owino, owinoalex55@gmail.com; Md. Yachin Islam, yachinislam@gmail.com; Zakaria Hossain, zakaria@bio.mie-u.ac.jp | ¹Graduate School of Bioresources, Mie University, Tsu City, Japan.



In chemical treatment for soil improvement, ground improvement is achieved by mixing various chemicals, for example, cement and lime, with soil to develop desirable characteristics [6]. These methods have shown a long-term change in ground properties. Still, some environmental concerns are usually associated with them [1, 5]. Cement serves as a crucial binding material in the construction industry [7]. However, it is characterized by its high cost, substantial energy consumption, depletion of natural resources, and significant emission of greenhouse gases into the atmosphere [8]. The production of one ton of cement results in approximately one ton of CO₂ gas emissions, leading to severe environmental contamination and various pollution-related issues [9]. Many studies have been conducted to search for cementitious [10], low-priced [11], readily available cement replacement materials from the cement industry to minimize greenhouse gases for environmental protection [12]. Predominantly, one of the cement replacement materials gaining research attention is rice husk ash made from rice husks, a product of rice milling [13]. As per FAOSTAT data from 2020 [14], the global paddy production reached 782 million tons in 2018. Extrapolating from this information, approximately 172 million tons of rice husks were generated that year, potentially producing 34 million tons of Rice husks (RHA) if all rice husks were incinerated [15]. However, due to underutilization, low market value, and logistical challenges in transportation, this substantial quantity of RHA is often indiscriminately disposed of in landfills, agricultural fields, riverbanks, [14] and open areas near populated regions. This unregulated disposal leads to air, soil, and water pollution, [16] releasing toxic substances and posing risks to public health.

RHA comprises the highest amount of amorphous silica among all agricultural wastes [14]. The content of SiO₂ in RHA is more than 70% [15], and it can go up to more than 90%, especially under controlled combustion temperature conditions [17, 18]. Moreover, the morphology of SiO₂ in RHA subjected to low-temperature combustion consists of nano-sized amorphous particles [16], which exhibit very high pozzolanic activity similar to silica fume [19]. This means that RHA has a potential gelling activity to promote the generation of cementitious hydration products as C–S–H/C–A–S–H under certain conditions [20]. Many researchers have discovered that adequately utilizing locally obtainable RHA as a pozzolanic material in ground improvement can decrease environmental degradation and construction price and increase soil strength properties [21]. The amorphous silica (SiO₂) in RHA chemically reacts with free calcium hydroxide Ca(OH)₂ in the secondary hydration reaction of cement [22] and forms the calcium silicate hydrate (C–S–H) gel, which improves the strength and durability of soil [23, 24]. Researchers have found that the utilization of RHA in construction projects can diminish CO₂ emissions by reducing the production of cement [25], waste disposal problems, environmental pollution, construction costs, and consumption of natural resources [26], and can increase the strength and durability of concrete and soil [27].

Additionally, RHA can effectively improve soil shear strength [28], indicating the potential for economic and environmental benefits [29]. Moreover, Incorporating RHA into geotechnical engineering practices allows us to contribute to a sustainable future by mitigating waste [30], reducing carbon emissions [31], and fostering the principles of sustainable development [32]. Furthermore, our study uniquely emphasizes minimal cement dosage, a distinguishing feature that differentiates it from the prevailing literature. Most existing research has primarily focused on the impact of combining rice husk ash with cement to enhance the cohesion of cohesionless soils, leaving exploring its effects on weak clay soils and subgrade utilization relatively underexplored [33–35]. This distinctive approach underscores our commitment to providing innovative solutions for sustainable ground improvement while efficiently managing construction materials, making it an essential contribution to the field. On the other hand, investigating subgrade layers and their influence on the overall shear strength of RHA-cement treated soils has remained a relatively unexplored area in the existing literature.

An experimental study was conducted to evaluate the shear strength of this new construction material. Sixteen specimen combinations of weak expansive with well-defined subgrade layers of soil-RHA-cement were investigated to understand the effects of RHA and cement on the shear strength parameters. The admixtures for each subgrade were prepared by mixing soil with 2%, 4%, and 6% RHA and 2%, 4%, and 6% cement. The upper, bottom, and subgrade double layers were used. A comprehensive analysis of the shear stress–shear displacement relationship, cohesion, and internal friction angle was done.

2 Materials and methods

2.1 Materials

2.1.1 Soil

The soil utilized in this study was collected from the Handa area, Tsu City, Mie Prefecture, Japan, located approximately 22 km away from Mie University. The exact location of soil sampling is shown in Fig. 1. The selection of this location was motivated by its characterization as an area facing challenges associated with weak, expansive, and loose soils.

Following standard geotechnical practices [36], systematic soil sampling was conducted to obtain representative samples. The soil used in this research was air-dried for three weeks [37] and then sieved through the 2 mm sieve [38] before the triaxial test. Air drying the soil for three weeks ensured the moisture content was consistent across all samples. This was crucial to obtaining more accurate, reproducible [39], and comparable test results, as inconsistent moisture content could lead to variations in soil behavior during testing. Sieving through the 2 mm sieve removed coarse particles and aggregates, ensuring that the soil used in the triaxial test was relatively homogeneous. This enhanced the accuracy of the test results [40] and ensured that the soil conforms to the specified particle size requirements and can be easily weighed, mixed, and compacted into the desired specimen shape for the triaxial test. Subsequently, various analyses were carried out, including sieve, hydrometer, liquid, and plastic limit analyses to classify the soil. The liquid and plastic limits of the soil were measured to be 48.5% and 28.594%, respectively. The soil composition comprised 0.02% sand, 57.28% silt, and 42.7% clay. According to the American Association of State Highway and Transportation Officials (AASHTO) classification, the soil was identified as A-7-6 (5) clayey soil. These soil characteristics indicate that it belongs to the category of clay soil. A detailed grain size analysis for soil, rice husk ash (RHA), and cement is presented in Fig. 2. Testing procedures followed Japan Industrial Standards JIS A 1204 [41] for the sieve and hydrometer test and JIS A 1205 [41] for the liquid and plastic limit tests. Additional geotechnical properties are detailed in Table 1.

2.1.2 Rice husk ash

A controlled burned RHA at 650–700°C with a high silica content of 91.10% was provided by Make Integrated Technology Co., Ltd, Osaka, Japan. The high silica content was obtained by burning the rice husks for 27 h in a computer-controlled self-combustion Ethical Star ash production machine. The RHA particle sizes ranged from 0.07 to 0.3 mm. Detailed particle size distribution of soil and RHA is shown in Fig. 2. A detailed physical and chemical property chart for rice husk ash is illustrated in Table 1.

Fig. 1 The exact location of soil sampling used in this study

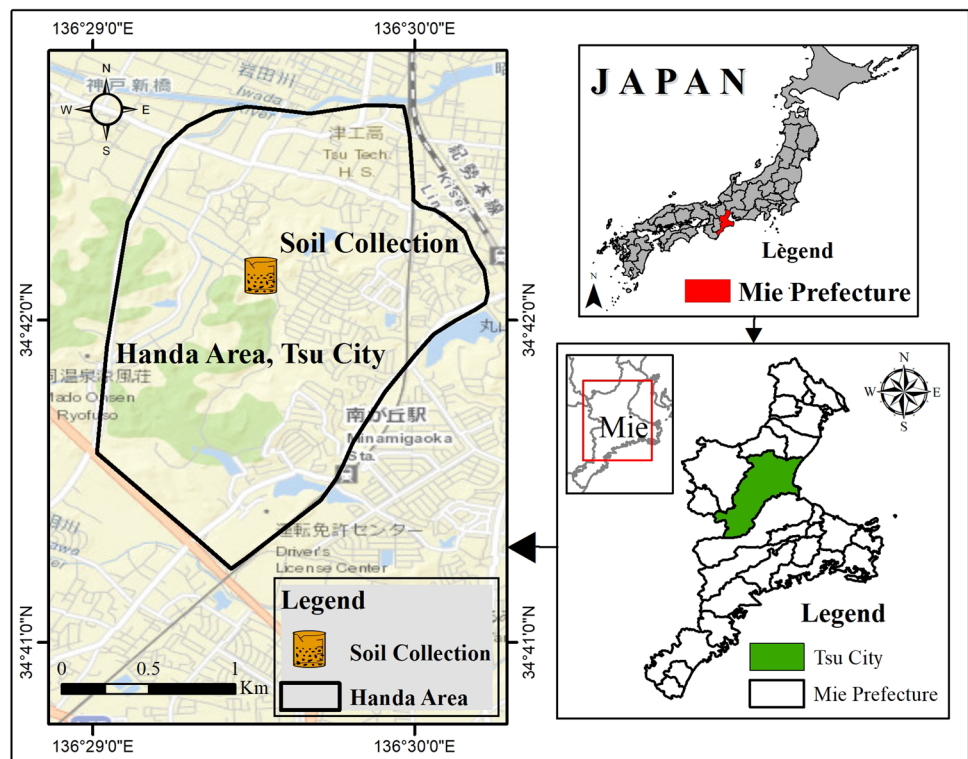


Fig. 2 Particle size distribution for Soil, Cement, and RHA

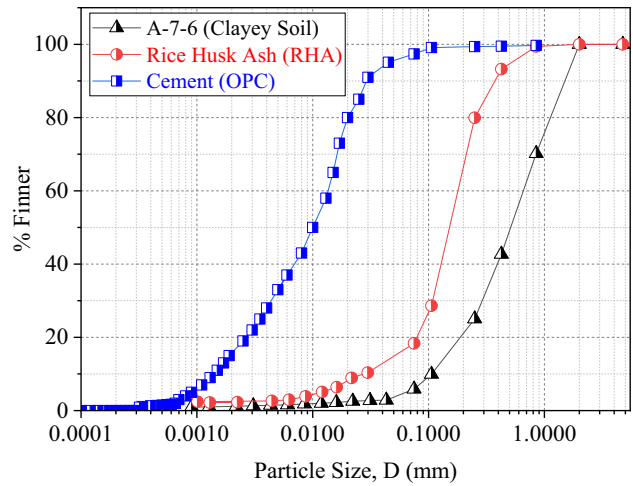


Table 1 Properties of Soil and RHA

Materials	Property	Value
Soil Properties	Specific gravity, g/cm ³	2.74
	Maximum dry density, g/cm ³	1.58
	Saturation, %	87.14
	Sand (75 µm—2 mm), %	0.02
	Silt (5–75 µm), %	57.28
	Clay < 5 µm, %	42.7
	Liquid limit, LL, %	48.5
	Plastic limit, PL, %	28.594
	Plasticity Index, PI, %	19.906
	AASHTO classification	A-7–6(5)
RHA Properties	Average Particle Size, mm	0.001 to 0.3
	Loss of Ignition, %	4–6
	Specific Gravity, g/cm ³	2.12
	Burning Temperature, °C	650–700
	Burning time, hour	27
	Silica (SiO ₂), %	91.10
	Carbon dioxide (CO ₂), %	4.35
	Potassium Oxide (K ₂ O), %	2.40
	Calcium Oxide (CaO), %	0.57
	Iron Oxide (Fe ₂ O ₃), %	0.05
	Alumina (Al ₂ O ₃), %	0.03
	Others, %	1.50

2.1.3 Portland cement

Ordinary Portland Cement (OPC) was also used as a binder element. The physical and chemical properties of OPC cement are illustrated in Table 2. [41]

2.2 Specimen preparation

A series of specimens were prepared using an experimental sample to investigate the effects of soil-RHA-cement mixtures on shear strength (Fig. 3a). The entire sample had a total weight of 500 g and a height of 12.5 cm. The weight of each specimen was determined by dividing the total weight of the sample by the height, resulting in a ratio of 40 g per 1 cm.

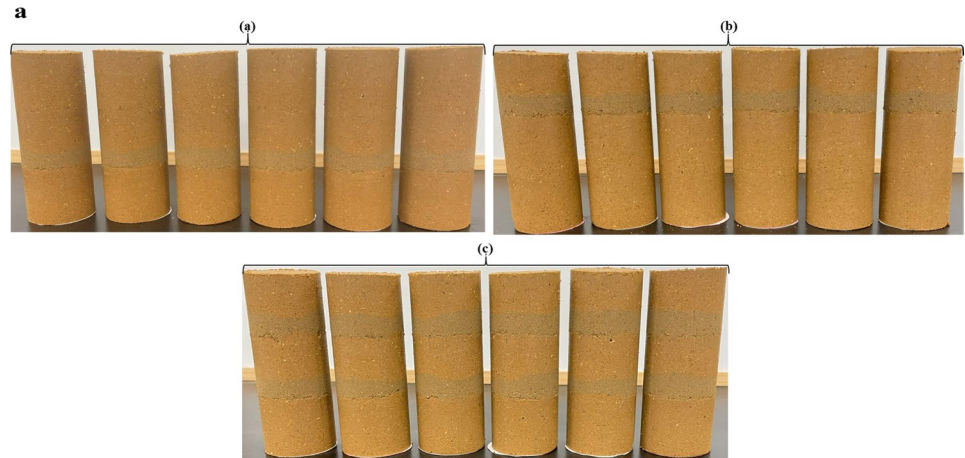
Approximately 160 g of soil was used for each specimen to form each layer. In the layer designated for experimentation, a mixture of 40 g of soil, RHA, and cement was added to 120 g of soil alone, creating a layer with a height of 1 cm composed explicitly of the soil-RHA-cement mixture to be tested (Fig. 3b). The specimens were manually compacted inside a mold with a height of 12.5 cm and a diameter of 5.0 cm. The compaction process involved compacting the specimens in three layers using a 4.9 cm diameter hand rammer with a mass of 1 kg. Each layer was compacted by applying 20 blows with a falling height of 30 cm. This ensured the uniform and consistent compaction of the soil-RHA-cement mixture within the specimens. The components were thoroughly mixed in a large tray to achieve a homogeneous mixture of soil-RHA-cement. Water was added gently to the dry mix, ensuring proper hydration without excessive saturation. The amount of water added to each specimen was determined based on the optimum moisture content (OMC). All testing procedures followed the Japan Industrial Standards (JIS) A 1210 standards [42] calculated from the compaction test. This meticulous specimen preparation and compaction method ensured the integrity and reliability of the subsequent shear strength testing using specific weight ratios and standardized compaction techniques.

In this study, the dosage of RHA was selected as 2%, 4%, and 6% based on the maximum utilization of amorphous silica at low percentages, as indicated by previous research [17, 41]. The maximum utilization of amorphous silica was 5%; therefore, we chose 2%, 4%, and 6% to investigate the effects of increasing the dosage by 1% and decreasing it by 1%. In addition, it is essential to highlight that this study primarily focuses on treating the soil to improve its properties while incorporating a small amount of cement 2%, 4%, and 6% [17, 28]. Including a minimal cement dosage complements the soil treatment process and ensures optimal proportions of Ca⁺ ions during pozzolanic reactions. This approach not only aligns with the objectives of environmental conservation and carbon emission reduction discussed in the introduction section but also emphasizes the soil treatment aspect of the study rather than focusing solely on concrete.

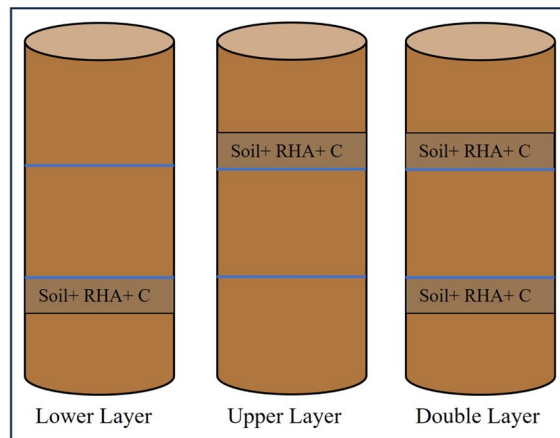
Table 2 Properties of OPC

Materials	Property	Value
Cement Properties	Initial setting time, minutes	170
	Final setting time, minutes	225
	Specific gravity, g/cm ³	3.15
	Specific surface area, m ² /kg	340
	28-day compressive strength, MPa	33–53
	Calcium Oxide (CaO), %	63.40
	Silicon dioxide (SiO ₂), %	21.60
	Iron Oxide (Fe ₂ O ₃), %	5.35
	Alumina (Al ₂ O ₃), %	4.45
	Sulfur trioxide (SO ₃), %	1.92
	Magnesium oxide (MgO), %	1.65
	Sodium oxide (Na ₂ O), %	0.11
	Potassium oxide (K ₂ O), %	0.22
Loss of ignition, %	< 4	

Fig. 3 **a** Specimen preparation for laboratory test (a) Lower layers, (b) Upper layers, (c) Double layers. **b** Specimen preparation for different layers



b



2.3 Testing method

2.3.1 Compaction test

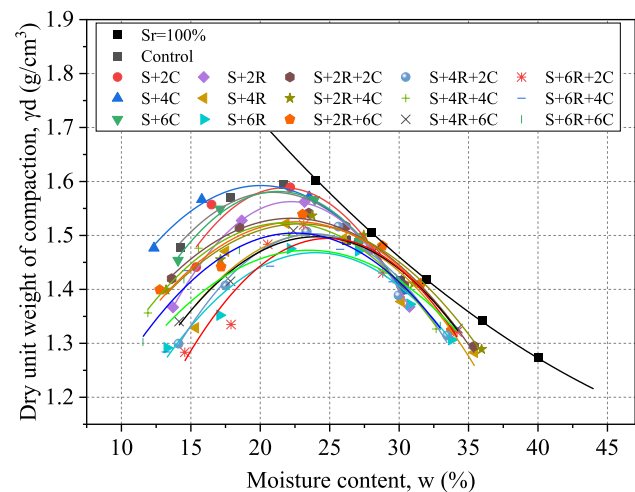
For each material blend shown in Table 3, a standard proctor compaction test was done to determine the optimum moisture content (w_{opt}) and the corresponding maximum dry density (ρ_{dmax}). Each blend was compacted into a cylindrical mold measuring 10 cm in diameter and 12.73 cm in height using a 2.5 kg rammer at a falling height of 30 cm while maintaining a constant compaction effort for each of the three layers. This process was repeated for various known moisture contents, and the dry densities were calculated for each. The plots of the dry density to the moisture content also called the compaction curves, were then used to obtain the peak points representing the maximum dry density and the optimum moisture content. All testing procedures followed the Japan Industrial Standards (JIS) A 1210 standards [42]. The results of optimum moisture content and dry density for soil and the soil blends are shown in Fig. 4.

2.3.2 Triaxial compression test

The experimental procedure followed the Japan Geotechnical Society 0520 ~ 0524 standards [17]. Consolidated drained (CD) triaxial tests were conducted on cylindrical specimens with a diameter of 5 cm and a height of 12.5 cm [43]. To prepare the specimens, each blend was compacted in three layers using a 1 kg rammer dropped

Table 3 Detailed blend combinations

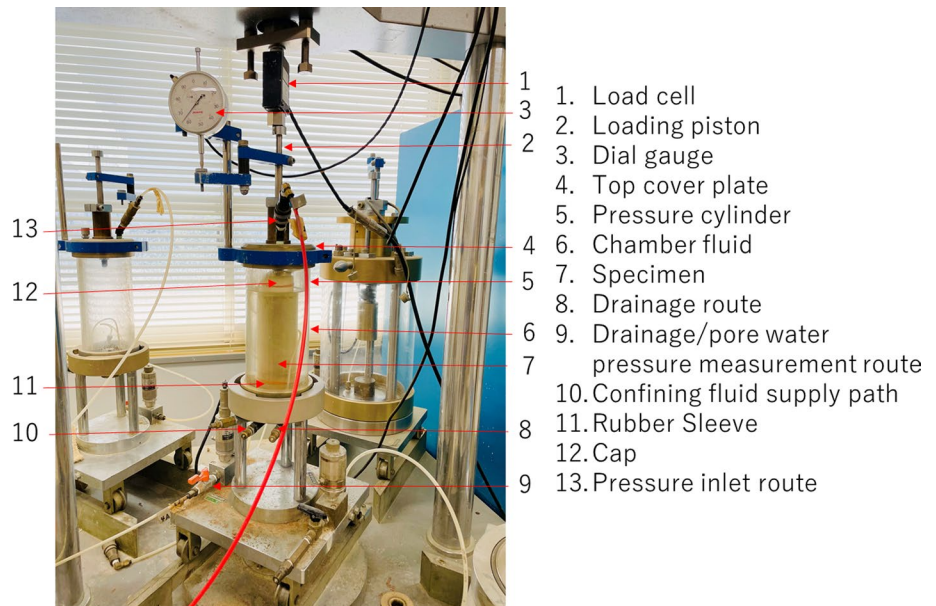
Blends	Soil, S (%)	RHA (%)	Cement, C (%)
Soil (Control)	100	0	0
S:2C	98	0	2
S:4C	96	0	4
S:6C	94	0	6
S:2R	98	2	0
S:4R	96	4	0
S:6R	94	6	0
S:2R:2C	96	2	2
S:2R:4C	94	2	4
S:2R:6C	92	2	6
S:4R:2C	94	4	2
S:4R:4C	92	4	4
S:4R:6C	90	4	6
S:6R:2C	92	6	2
S:6R:4C	90	6	4
S:6R:6C	88	6	6

Fig. 4 Effects of RHA and cement on compaction characteristics

from a height of 30 cm into a mold of similar dimensions. The specimens were then placed in the triaxial test pressure chamber and sealed with a rubber sleeve, as depicted in Fig. 4. The experimental setup for the consolidated drained triaxial tests included several key components: (1) a load cell for measuring the axial load, (2) a loading piston to apply axial loading on top of the specimen, (3) a dial gauge for measuring axial displacement, (5) a pressure cylinder to hold the chamber fluid, (6) chamber fluid to exert hydrostatic chamber pressure (σ_3), (9) a route for measuring drainage/pore water pressure, (10) a path for supplying the confining fluid, and (13) an inlet for air pressure. Figure 5 provides a detailed illustration with labeled components.

This study used three confining pressures: 50 kPa, 100 kPa, and 150 kPa. The drainage/pore water pressure measurement route was kept open to ensure a drained condition within the specimen, preventing the development of pore water pressure within the composite structure. Shearing the specimens occurred slowly at a rate of 0.5 mm/min. Deviatoric stresses and axial strains were recorded throughout the experiment using a data logger. The experiment was terminated when the peak deviatoric stress value was reached or the axial strain got two-thirds or 10% of its initial value, whichever occurred first.

Fig. 5 Triaxial testing apparatus



2.3.3 Microstructural study on shear strength development

A comprehensive investigation of shear strength development in the reinforced and Treated soil composite necessitated using microstructural analysis techniques, including scanning electron microscopy (SEM) imaging and Energy-Dispersive X-ray Spectroscopy (EDS). SEM imaging was a critical tool to examine the soil composite at a micrometer scale. It utilized low-energy secondary and backscattered electrons to visualize the structural alterations occurring within the new composite material [44]. The three-dimensional images produced by the SEM test effectively portrayed the influence of additives in modifying the surface morphology of the stabilized soil at a micro-level [45, 46]. EDS, on the other hand, played a pivotal role in identifying crystalline patterns, offering a comprehensive analysis of the extent to which chemical stabilizing agents were incorporated into the treated soil composite. More specifically, EDS facilitated a deeper comprehension of the various chemical transformations in the treated soil due to pozzolanic reactions [47–49].

Fig. 6 The relationship between axial strain and specimen combination for the lower layer

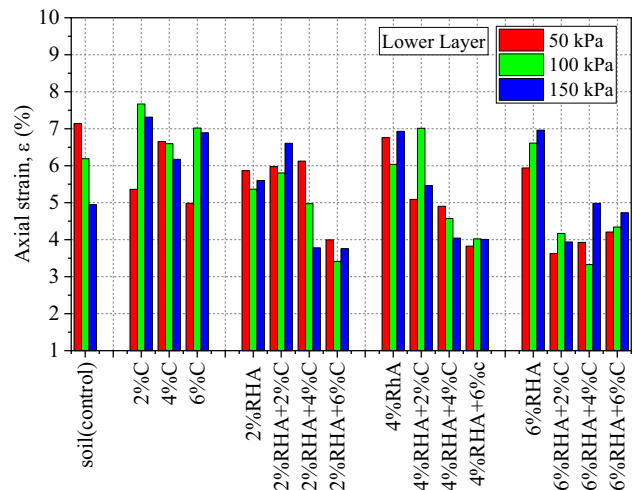


Fig. 7 The relationship between axial strain and specimen combination for the Upper layer

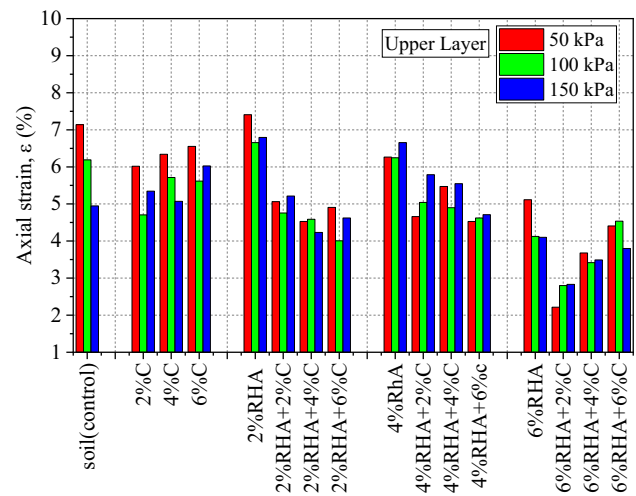
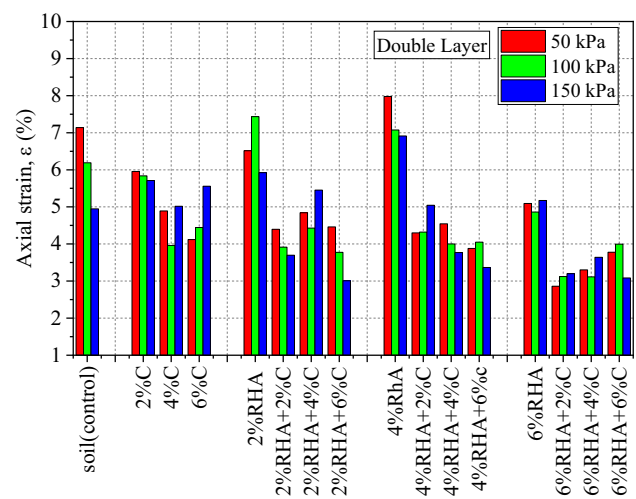


Fig. 8 The relationship between axial strain and specimen combination for the Double-layer



3 Results and discussion

3.1 The relationship between axial strain, deviatoric stress, and specimen combination

Figures 6, 7, and 8 depict the correlation between axial strain and specimen combinations for the lower, upper, and double layers. These combinations consisted of varying percentages (2%, 4%, 6%) of RHA and (2%, 4%, 6%) cement. When 2% cement was added to the lower and double layers, the axial strain ranged from 6 to 7%. By increasing the cement content to 4%, the axial strain decreased to 5% for the double layer and 6% for the lower layer. Notably, with 6% cement, the axial strain was slightly increased across all sub-grade layers. On the other hand, focusing on specimens containing RHA alone, the axial strains slightly increased to 7% due to the compressibility of the porous RHA microstructure. However, 2% to 6% of cement content reduced axial strains by 4% for all subgrade layers, attributed to the formation of cementitious compounds within the specimen structure.

Figures 9, 10, and 11 illustrate the correlation between deviatoric stress and specimen combinations for the lower, upper, and double layers. The results demonstrated a clear trend of increasing deviatoric stresses with higher confining pressures ranging from 50 to 150 kPa. In this study, the double-layered specimens exhibited the highest deviatoric stresses compared to the lower and upper layers. For instance, when examining the specimen with a combination of 2% RHA and 6% Cement (2%RHA6%C), the double layer achieved maximum deviatoric stresses of 383 kN/m². In contrast, the lower and upper layers attained 368 kN/m² and 338 kN/m², respectively. The outstanding increase in deviatoric stresses can be attributed to the improved resistance to deformation resulting from the pozzolanic reactions between RHA and cement, as discussed in the introduction, a phenomenon corroborated by findings similar

Fig. 9 The relationship between Deviatoric stress and specimen combination for the Lower layer

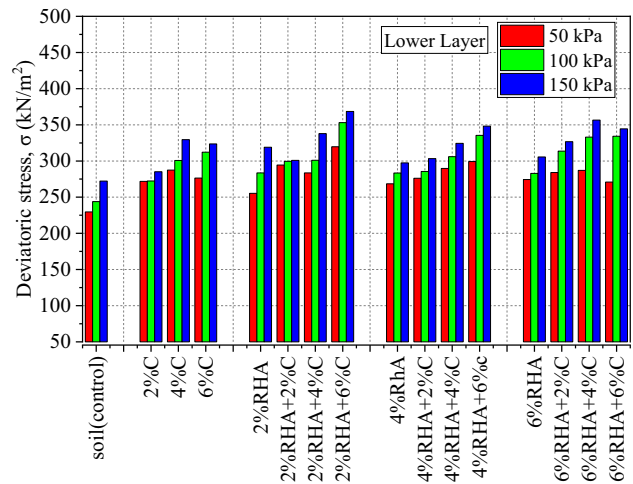


Fig. 10 The relationship between Deviatoric stress and specimen combination for the Upper layer

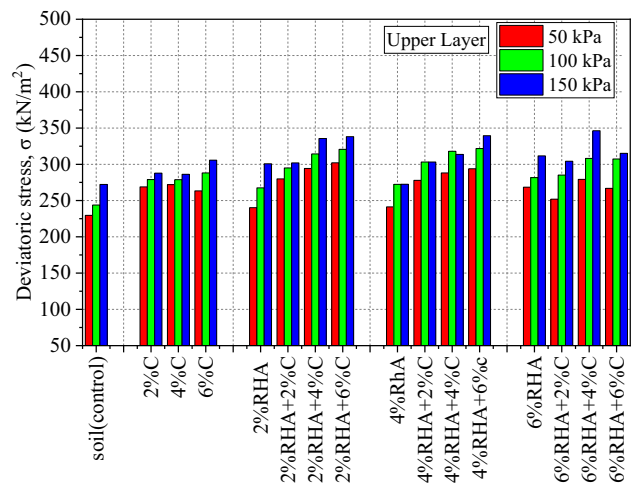
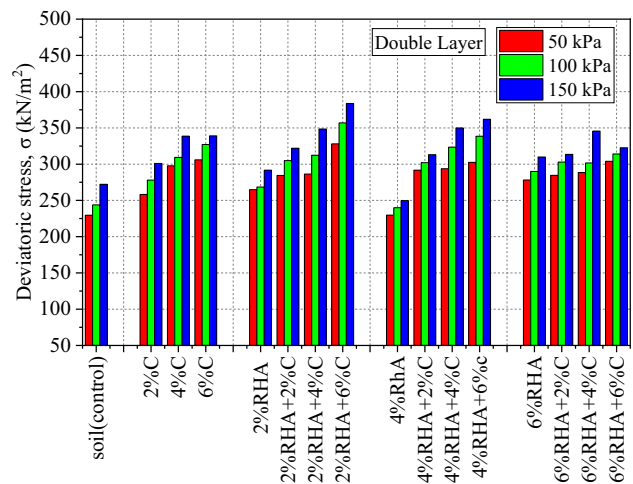
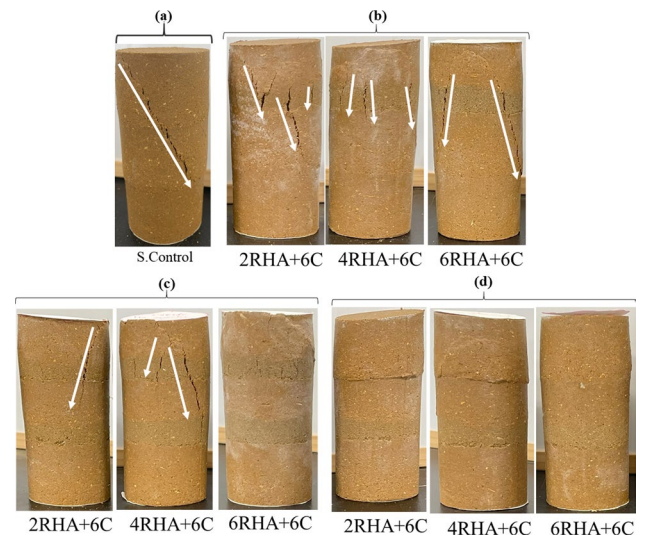


Fig. 11 The relationship between Deviatoric stress and specimen combination for the Double-layer



to those reported by Rachmawati [28]. Introducing 2% RHA across all the specimen combinations led to improved deviatoric stresses for all subgrade layers compared to the control specimens and those with cement only. However, a slight reduction in deviatoric stresses was observed as the RHA content increased from 2 to 6%, specifically in the double layer.

Fig. 12 Specimens failure planes at 150 kPa confining pressure **a** Soil control, **b** Upper layers, **c** Double layers, **d** Lower layers



In conclusion, the highest deviatoric stresses were achieved by the double layer in the specimen containing 2% RHA and 6% cement, as evident from Fig. 11. Furthermore, in our quest to comprehend how unreinforced and RHA-Cement-reinforced specimens respond mechanically to shear, we harnessed photographic data that unveils the failure patterns during testing. These revealing visuals are illustrated in Fig. 12.

Notably, it proved intriguing that the composition of RHA and Cement within this subgrade soil significantly influenced the initiation points of failure cracks. Consequently, the position from which these cracks emanate hinges primarily on the arrangement of RHA-Cement mixtures and the number of layers. For instance, when one layer of 2RHA + 6C or 4RHA + 6C is embedded in the upper layer, the fractures are observed to initiate solely within the upper region and propagate towards the middle, as depicted in Fig. 12b. Additionally, incorporating 6RHA + 6C in the upper layer similarly results in fractures originating in the upper section and extending into the lower layer, as presented in Fig. 12b. However when double layers of 2RHA + 6C and 4RHA + 6C are embedded, this zone doesn't exhibit the same level of reinforcement, thus leading to fractures starting in the weaker upper portion and extending into the middle soil layers, as indicated in Fig. 12c. Conversely, embedding 6RHA + 6C in the double layers produces a robustly stiffened zone.

On the contrary, a notable reduction in visible vertical planes of weakness (cracks) within the lower layers is observed when embedding in the lower layer, as evidenced in Fig. 12d. This decrease emphasizes the existence of augmented elasticity within the specimens, consistent with similar outcomes reported in other studies [19, 31]. They affirmed the RHA-cement composite's effectiveness in curbing cracks within RHA-cement composite soil composites.

Fig. 13 The relationship between the angle of internal friction (ϕ) and specimen combination for the Lower layer

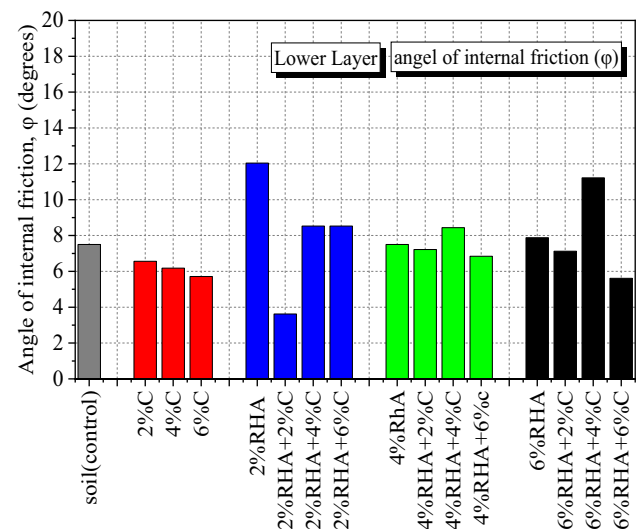


Fig. 14 The relationship between the angle of internal friction (ϕ) and specimen combination for the Upper layer

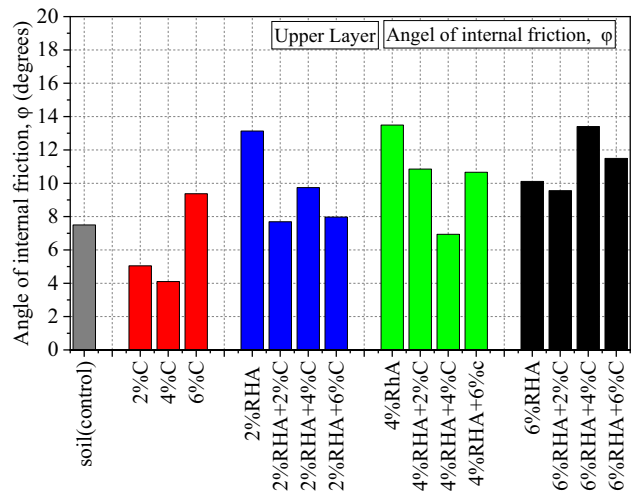


Fig. 15 The relationship between the angle of internal friction (ϕ) and specimen combination for the Double layer

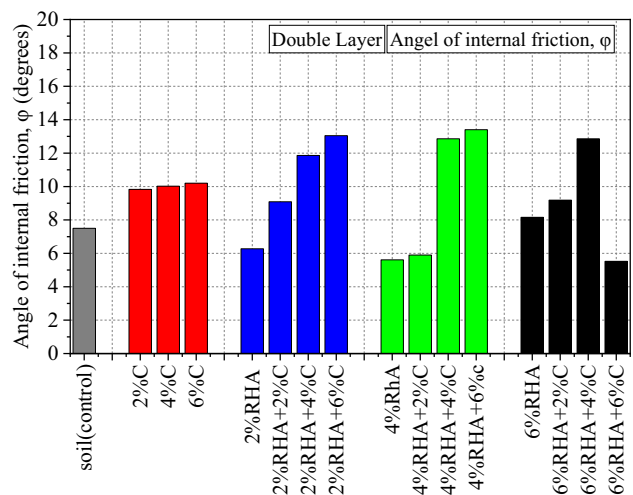
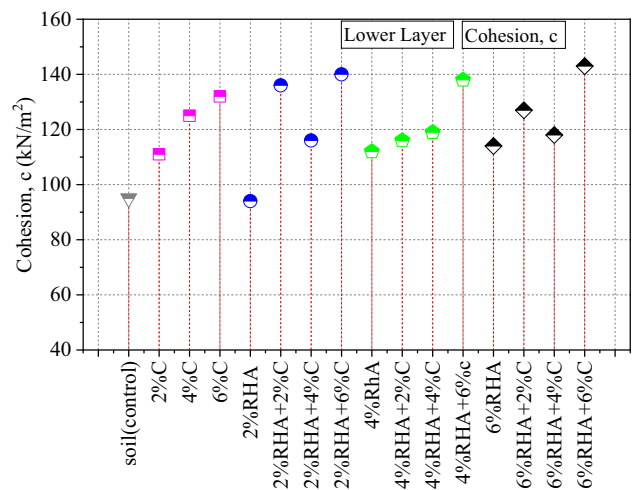


Fig. 16 The relationship between the cohesion (c) and specimen combination for the Lower layer



3.2 Effects of RHA and cement subgrade layers on shear strength parameters

The present study aimed to quantify the shear parameters of the stabilized expansive soil using the Mohr–Coulomb failure theory, which describes the relationship between shear stress (τ) and effective normal stress (σ). The shear

Fig. 17 The relationship between the cohesion (c) and specimen combination for the Upper layer

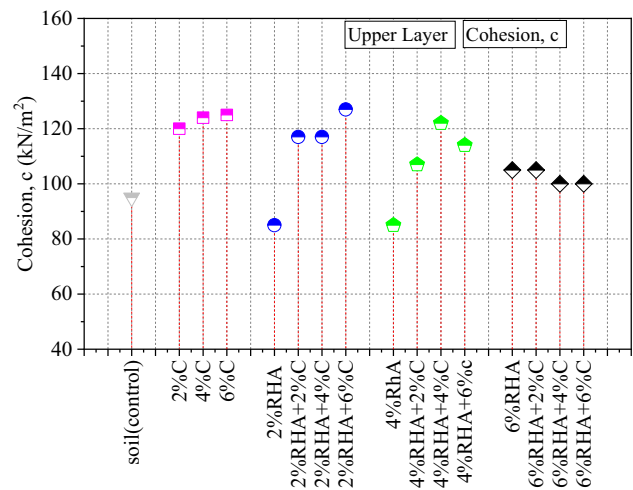
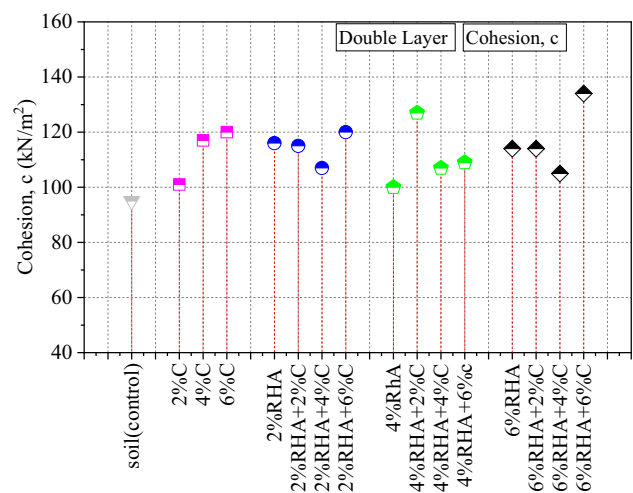


Fig. 18 The relationship between the cohesion (c) and specimen combination for the Double layer



strength parameters regarding the angle of internal friction (ϕ) are summarized in Figs. 13, 14, and 15. Incorporating RHA and cement resulted in an enhanced angle of internal friction for the soil-RHA-cement composite in the lower Fig. 13 and double subgrade layers Fig. 15. This improvement can be attributed to the irregular shapes formed during the pozzolanic reactions between RHA and cement particles, which contributed to increased frictional resistance within these layers of the specimens. However, slight variations in the angle of internal friction were observed, specifically in the lower layers. These differences can be attributed to the location of the subgrade layer within the specimen, as the shear plane was positioned well above the subgrade layer.

The shear strength parameters were also presented, as shown in Figs. 16, 17, and 18. Concerning the cohesive strength observed in all the examined specimens, it is noteworthy that the inclusion of cement and RHA exerted a substantial impact compared to the control, aligning with findings akin to those reported by other studies [41, 50]. The highest cohesion values were achieved with 6% cement, particularly demonstrating eminent advancements in the lower Fig. 16 and double subgrade layers Fig. 18. For instance, specimens 6%RHA6%C, 4%RHA6%C, and 2%RHA6%C exhibited cohesion values of 143 kN/m², 138 kN/m², and 140 kN/m², respectively, as shown in Fig. 16. Similarly, specimen 6%RHA6%C attained the highest cohesive strength when considering the double subgrade layer with a value of 134 kN/m², as depicted in Fig. 18.

Figure 17 shows a slight reduction in the cohesion value across all the specimen combinations. This observation suggests that the upper subgrade layer possessed the lowest cohesion values, indicating weaker bonding between its particles and the composition of the subgrade. It is worth noting that this layer was located along the shear plane, thereby experiencing direct initial contact with the axial load.

Fig. 19 SEM image for Soil-only specimen at $\times 500$

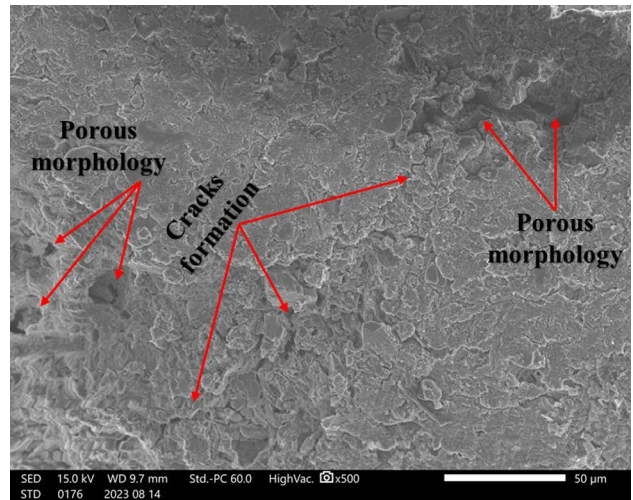


Fig. 20 SEM image for 2RHA + 6C specimen at $\times 500$

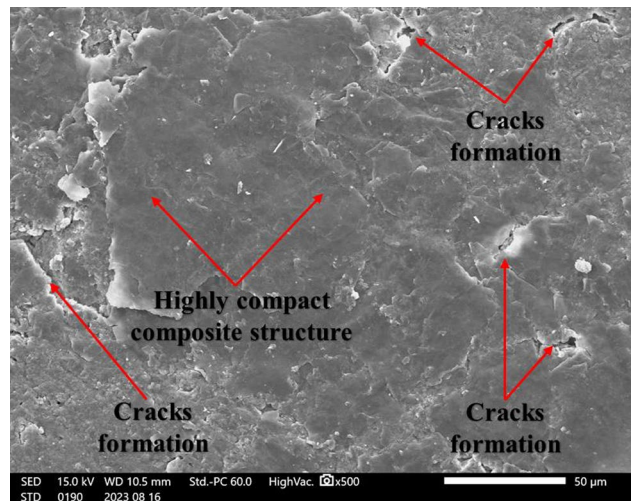


Fig. 21 SEM image for 4RHA + 6C specimen at $\times 500$

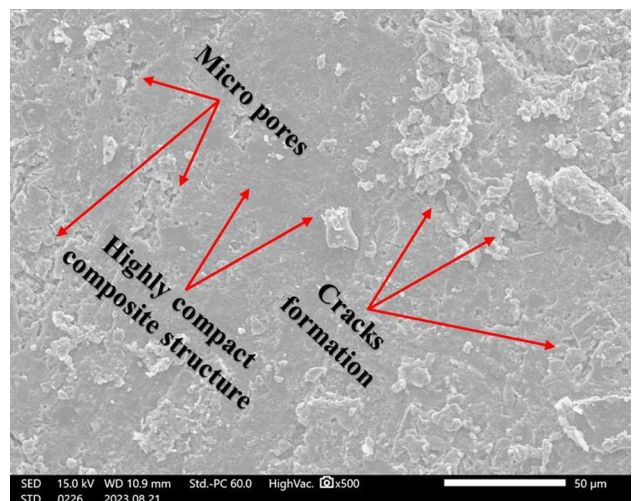


Fig. 22 SEM image for 6RHA + 6C specimen at $\times 500$

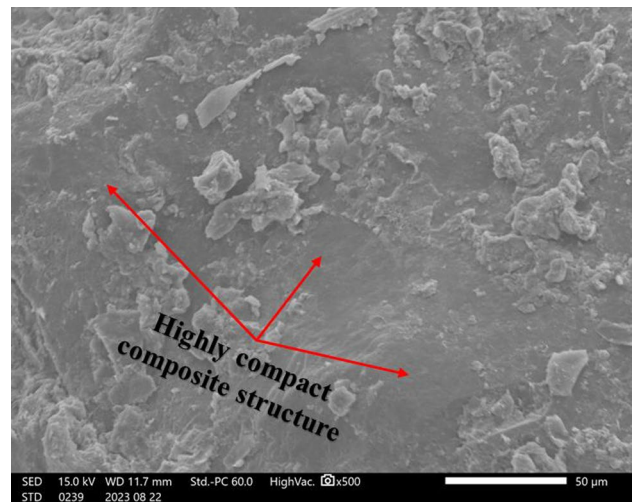


Fig. 23 EDS spectrum of soil and its elemental composition

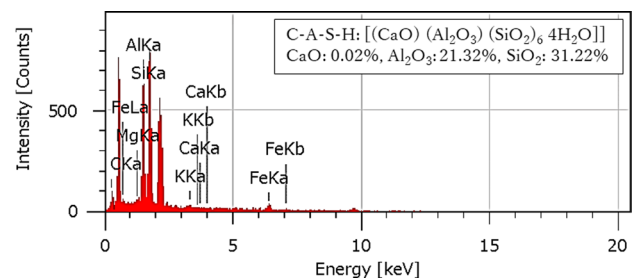


Fig. 24 EDS spectrum of 2RHA6C and its elemental composition

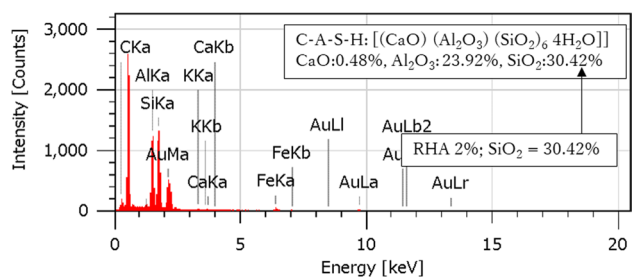
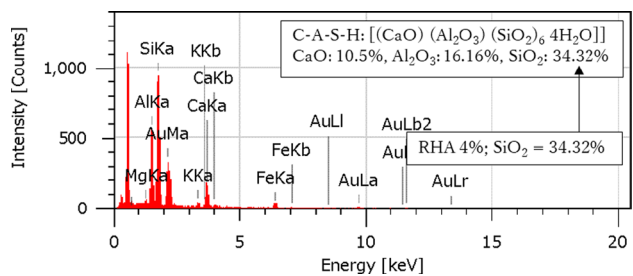


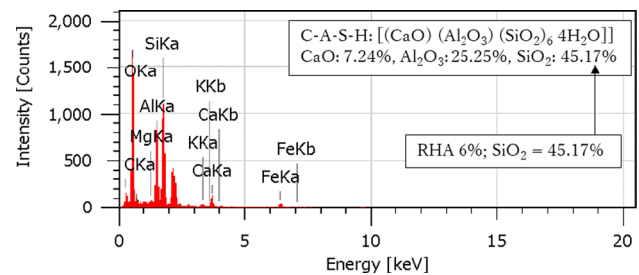
Fig. 25 EDS spectrum of 4RHA6C and its elemental composition



3.3 SEM and EDS analysis

In this study, incorporating a mixture comprising RHA, cement, and soil impacted the failure behavior under shear forces. Therefore, it is essential to comprehend the reinforcing mechanism to substantiate their potential in preventing the formation of weak planes within the composite materials. To begin with, we conducted a microstructural

Fig. 26 EDS spectrum of 6RHA6C and its elemental composition



analysis to illustrate the structural alterations in specimens containing only soil. Subsequently, we examined the overall composite structure after introducing RHA and cement. It became apparent that micro-cracks formation was a common occurrence in the unreinforced specimens. Porous morphology (micro-pores) and micro-cracks indicated an increased susceptibility to shear failure during loading due to the proliferation of weak planes, as depicted in Fig. 19 for the control sample (S Control). However, for the samples containing 2RHA + 6C and 4RHA + 6C, as shown in Figs. 20 and 21, there was a notable reduction in micro-crack formation and the development of a more cohesive cemented composite structure. Furthermore, adding modest amounts of cement and RHA (6RHA + 6C) enhanced the degree of cementation within the composite structure, decreasing the development of micro-pores and micro-cracks, as illustrated in Fig. 22. Other relevant studies have reported similar findings [51].

The specimens underwent EDS analysis to determine their elemental chemical composition and relative abundance. Figures 23, 24, 25, 26 present the EDS spectra and elemental compositions of the soil, 2RHA6C, 4RHA6C, and 6RHA6C samples. The influence of introducing RHA and cement as stabilizing agents is apparent in these figures. As the RHA content increased, there was a corresponding increase in the SiO_2 percentage because RHA is rich in SiO_2 . This is evident from the higher SiO_2 levels in the EDS graphs when RHA increased from 2 to 6%. When the RHA content is increased with cement, a substantial amount of C–S–H (calcium–silicate–hydrate) gel formation is observed. This C–S–H gel formation can be attributed to the pozzolanic activity between RHA, cement, and soil. Interestingly, it was observed that Aluminum ions were incorporated into the C–S–H gel. This Aluminum ion uptake occurred both on the surface and in the inter-layer of the gel, leading to the formation of stronger C–A–S–H gel bonds referred to as Calcium Alumino Hexasilicate Tetrahydrate $[(\text{CaO})(\text{Al}_2\text{O}_3)(\text{SiO}_2)_6 4(\text{H}_2\text{O})]$, as illustrated in Figs. 25 and 26. Other pertinent research has documented comparable outcomes [41, 52, 53].

4 Conclusion

This paper comprehensively investigated the effects of incorporating RHA and cement into clay soils as subgrade layers, shedding light on their mechanical behavior and microstructural characteristics. Sixteen samples were meticulously examined through triaxial tests, and the results were thoughtfully analyzed in terms of deviatoric stress, axial strain, angle of internal friction (ϕ), and cohesion (c). Meanwhile, the double layer achieved maximum deviatoric stresses of 383 kN/m^2 in the specimen (2%RHA6%C). Remarkably, the angle of internal friction exhibited a noticeable increase with higher RHA-Cement content in the subgrade layer. This observed phenomenon can be attributed to the pozzolanic reactions within the subgrade, contributing to increased friction and enhanced interlocking between soil particles. It is essential to note that conventional triaxial test results supported these outcomes and were consistent with the SEM analysis, which provided valuable insights into the microstructural changes occurring within the subgrade layers. The SEM analysis revealed the development of distinct structures and bonds due to the RHA-Cement treatment, corroborating the observed increase in the angle of internal friction.

Furthermore, the increase in cohesion, a critical parameter for soil improvement, was particularly pronounced in the lower subgrade layer. Specimen 6%RHA6%C demonstrated the highest cohesive strength with cohesion values of 143 kN/m^2 , compared to the soil control 95 kN/m^2 , corroborated by our EDS analysis, which provided elemental composition data supporting the enhanced cohesion. These findings underline the effectiveness of our innovative subgrade construction material comprising 6%RHA6%C, 4%RHA6%C, and 2%RHA6%C for sustainable ground improvement projects, a conclusion reinforced by both mechanical testing and the complementary SEM and EDS analyses. This comprehensive approach enhances our understanding of the material and demonstrates its potential to revolutionize the field of geotechnical engineering by combining mechanical performance with microstructural insights.

Acknowledgements The authors would like to acknowledge the Ph.D. Development Support for providing financial support (Fellowship) through Mie University, where this study was conducted. This research was also supported by Make Integrated Technology Limited (MIT), which provided experimental materials.

Author contributions AEA: Conceptualization, Methodology, Data curation, Writing- Original draft. AO: Reviewing, Data analysis. MYI: Reviewing, Formatting. ZH: Supervising, Reviewing.

Data availability Data will be made available on request.

Declarations

Competing interests The authors declare that they have no known competing financial interests or personal relationships that could have appeared to influence the work reported in this paper.

Open Access This article is licensed under a Creative Commons Attribution 4.0 International License, which permits use, sharing, adaptation, distribution and reproduction in any medium or format, as long as you give appropriate credit to the original author(s) and the source, provide a link to the Creative Commons licence, and indicate if changes were made. The images or other third party material in this article are included in the article's Creative Commons licence, unless indicated otherwise in a credit line to the material. If material is not included in the article's Creative Commons licence and your intended use is not permitted by statutory regulation or exceeds the permitted use, you will need to obtain permission directly from the copyright holder. To view a copy of this licence, visit <http://creativecommons.org/licenses/by/4.0/>.

References

1. Verma H, Ray A, Rai R, Gupta T, Mehta N. Ground improvement using chemical methods: a review. *Heliyon*. 2021. <https://doi.org/10.1016/j.heliyon.2021.e07678>.
2. Rachmawati SH, Hossain Z, Shiao J. Ground improvement using waste shell for farm roads and embankments. *J Agric Eng*. 2018. <https://doi.org/10.4081/jae.2018.731>.
3. Khazaei J, Moayedi H. Soft expansive soil improvement by eco-friendly waste and quick lime. *Arabian J Sci Eng*. 2019. <https://doi.org/10.1007/s13369-017-2590-3>.
4. Ikeagwuani CC, Nwonu DC. Emerging trends in expansive soil stabilisation: a review. *J Rock Mech Geotechn Eng*. 2019. <https://doi.org/10.1016/j.jrmge.2018.08.013>.
5. Afrin H. A review on different types soil stabilization techniques. *Int J Transport Eng Technol*. 2017. <https://doi.org/10.11648/j.ijtet.20170302.12>.
6. Dormohamadi M, Reza R. Combined effect of compaction and clay content on the mechanical properties of adobe brick. *Case Stud Construction Mater*. 2020. <https://doi.org/10.1016/j.cscm.2020.e00402>.
7. Jahanbakhsh H, Karimi MM, Naseri H, Nejad FM. Sustainable asphalt concrete containing high reclaimed asphalt pavements and recycling agents: Performance assessment, cost analysis, and environmental impact. *J Clean Prod*. 2020. <https://doi.org/10.1016/j.jclepro.2019.118837>.
8. Rokhmad A. Configuration and the role of community leaders in the conflict of natural resources of limestone mining for the cement industry in Rembang Indonesia. *Int J Energy Econ Policy*. 2020. <https://doi.org/10.32479/ijeeep.8321>.
9. Wei Y, Hadigheh SA. Cost benefit and life cycle analysis of CFRP and GFRP waste treatment methods. *Construct Build Mater*. 2022. <https://doi.org/10.1016/j.conbuildmat.2022.128654>.
10. Luhari I, Luhari S, Abdullah MMAB, Sandu AV, Vizureanu P, Razak RA, Imjai T. Solidification/stabilization technology for radioactive wastes using cement: an appraisal. *Materials*. 2023. <https://doi.org/10.3390/ma16030954>.
11. Hilal N, Doha MAS, Mohammed TK. Effect of egg shell ash and strap plastic waste on properties of high strength sustainable self-compacting concrete. *Arab J Geosci*. 2021. <https://doi.org/10.1007/s12517-021-06654-x>.
12. Lamb WF, Wiedmann T, Pongratz J, Andrew R, Crippa M, Olivier JG, Minx JA. A review of trends and drivers of greenhouse gas emissions by sector from 1990 to 2018. *Environ Res Lett*. 1990. <https://doi.org/10.1088/1748-9326/abee4e>.
13. Chen R, et al. Sustainable utilization of biomass waste-rice husk ash as a new solidified material of soil in geotechnical engineering: a review. *Construct Building Mater*. 2021. <https://doi.org/10.1016/j.conbuildmat.2021.123219>.
14. Nahar N, et al. Effects of controlled burn rice husk ash on geotechnical properties of the soil. *J Agric Eng*. 2021. <https://doi.org/10.4081/jae.2021.1216>.
15. Ahmad J, Rosli MIF, Abdul R, Abdul S. The Effect of Rice Husk Ash (RHA) Mixtures on Geotechnical Properties of Soil. In: *Regional Conference on Science, Technology and Social Sciences (RCSTSS 2016) Theoretical and Applied Sciences*. Springer Singapore. 2018; https://doi.org/10.1007/978-981-13-0074-5_33
16. Luhari I, Luhari S. A comprehensive review on fly ash-based geopolymer. *J Composites Sci*. 2022. <https://doi.org/10.3390/jcs6080219>.
17. Nahar N, Hossain Z, Tamaki N. Optimum utilization of rice husk ash waste for ground improvement. *Int Agric Eng J*. 2021;30:1–10.
18. Das SK, Adedirani A, Kaze CR, Mustakim SM, Leklou N. Production, characteristics, and utilization of rice husk ash in alkali activated materials: An overview of fresh and hardened state properties. *Constr Build Mater*. 2022. <https://doi.org/10.1016/j.conbuildmat.2022.128341>.
19. Abolhasani A, Samali B, Dehestani M, Libre NA. Effect of rice husk ash on mechanical properties, fracture energy, brittleness and aging of calcium aluminate cement concrete. 2022. <https://doi.org/10.1016/j.istruc.2021.11.054>.
20. Faried AS, Mostafa SA, Tayeh BA, Tawfik TA. The effect of using nano rice husk ash of different burning degrees on ultra-high-performance concrete properties. *Constr Build Mater*. 2021. <https://doi.org/10.1016/j.conbuildmat.2021.123279>.
21. Devi K, Kumar ACA. Soil improvement using waste materials: A review. *J Build Mater Sci*. 2020. <https://doi.org/10.30564/jbms.v2i1.2641>.

22. Jittin V, Minnu SN, Bahurudeen A. Potential of sugarcane bagasse ash as supplementary cementitious material and comparison with currently used rice husk ash. *Constr Build Mater*. 2021. <https://doi.org/10.1016/j.conbuildmat.2020.121679>.
23. Amran M, Fediuk R, Murali G, Vatin N, Karelina M, Ozbakkaloglu T. ... & Mishra. J Rice husk ash-based concrete composites: A critical review of their properties and applications. 2021. <https://doi.org/10.3390/cryst11020168>.
24. Ferretti E, Moretti M, Chiusoli A, Naldoni L, De Fabritiis F, Visonà M. Rice-Husk Shredding as a Means of Increasing the Long-Term Mechanical Properties of Earthen Mixtures for 3D Printing. 2022; <https://doi.org/10.3390/ma15030743>.
25. Wong JKH, Kok ST, Wong SY. Cementitious, pozzolanic and filler materials for DSM binders. *Civ Eng*. 2020. <https://doi.org/10.28991/cej-2020-03091479>.
26. Adamu M, Ayeni KO, Haruna SI, Mansour YEHI, Haruna S. Durability performance of pervious concrete containing rice husk ash and calcium carbide: A response surface methodology approach. *Case Stud Construction Materials*. 2021. <https://doi.org/10.1016/j.cscm.2021.e00547>.
27. Zerihun B, Yehualaw MD, Vo DH. Effect of Agricultural Crop Wastes as Partial Replacement of Cement in Concrete Production. *Advances in Civil Engineering*. 2022. <https://doi.org/10.1155/2022/5648187>.
28. Rachmawati SH, Hossain Z, Shiau J. Shear strength of soil by using clam shell waste as recycle aggregate. *J Agric Eng*. 2020. <https://doi.org/10.4081/jae.2020.1043>.
29. Tayeh BA, Alyousef R, Abduljabbar H, Alaskar A. Recycling of rice husk waste for a sustainable concrete: a critical review. *J Clean Prod*. 2021. <https://doi.org/10.1016/j.jclepro.2021.127734>.
30. Ahmad W, Ahmad A, Ostrowski KA, Aslam F, Joyklad P. A scientometric review of waste material utilization in concrete for sustainable construction. *Case Stud Construction Mater*. 2021. <https://doi.org/10.1016/j.cscm.2021.e00683>.
31. Hossain SS, Roy PK, Bae CJ. Utilization of waste rice husk ash for sustainable geopolymer: a review. *Constr Build Mater*. 2021. <https://doi.org/10.1016/j.conbuildmat.2021.125218>.
32. Eliaslankaran Z, Daud NNN, Yusoff ZM, Rostami V. Evaluation of the effects of cement and lime with rice husk ash as an additive on strength behavior of coastal soil. *Materials*. 2021. <https://doi.org/10.3390/ma14051140>.
33. Chen R, Congress SSC, Cai G, Zhou R, Xu J, Duan W, Liu S. Evaluating the effect of active ions on the early performance of soft clay solidified by modified biomass waste-rice husk ash. *Acta Geotech*. 2023. <https://doi.org/10.1007/s11440-022-01630-5>.
34. Onyelowe KC, Kontoni DPN, Ebid AM, Dabbaghi F, Soleymani A, Jahangir H, Nehdi ML. Multi-objective optimization of sustainable concrete containing fly ash based on environmental and mechanical considerations. *Buildings*. 2022. <https://doi.org/10.3390/buildings12070948>.
35. Ganasen N, Bahrami A, Loganathan K. A scientometric analysis review on agricultural wastes used as building materials. *Buildings*. 2023. <https://doi.org/10.3390/buildings13020426>.
36. Okalebo JR, Gathua KW, Woomeer PL. Laboratory methods of soil and plant analysis: a working manual. *Sacred Africa Nairobi*. 2002;21:25–6.
37. Obalum SE, Chibuike GU. Air-drying effect on soil reaction and phosphorus extractability from upland-lowland tropical soils as related to their colloidal stability. *Appl Ecol Environ Res*. 2017. https://doi.org/10.15666/aer/1501_525540.
38. Owino A, et al. Dimensional influence of basalt fiber reinforcements on the consolidation behaviour of rice husk ash stabilized soils. *Construct Build Mater*. 2022. <https://doi.org/10.1016/j.conbuildmat.2022.127686>.
39. Erich MS, Hoskins BR. Effects of soil drying on soil pH and nutrient extractability. *Commun Soil Sci Plant Anal*. 2011. <https://doi.org/10.1080/00103624.2011.566961>.
40. Haluschak P. Laboratory methods of soil analysis. *Canada-Manitoba soil survey*. 2006;3:133.
41. Owino AO, Hossain Z. The influence of basalt fiber filament length on shear strength development of chemically stabilized soils for ground improvement. *Constr Build Mater*. 2023. <https://doi.org/10.1016/j.conbuildmat.2023.130930>.
42. JIS A 1210. (In Japanese). Test method for soil compaction using a rammer. *Japanese Industrial Standard, Guidance and Basic - Soil Test*, The Jpn. Geotech. Soc. 2010; pp 71–78.
43. JGS 0524, (In Japanese). Method for consolidated-drained triaxial compression test on soils, *Jpn. Geotech. Soc. Dositsu Shiken Hou Dositsu Kogakkai*. 2001;pp233–43.
44. POLO-MENDOZA, Rodrigo, et al. Ultraviolet ageing of bituminous materials: A comprehensive literature review from 2011 to 2022. *Construction and Building Materials*. 2022; <https://doi.org/10.1016/j.conbuildmat.2022.128889>.
45. Cheraghian G, Wistuba M. Ultraviolet aging study on bitumen modified by a composite of clay and fumed silica nanoparticles. *Sci Rep*. 2020. <https://doi.org/10.1038/s41598-020-68007-0>.
46. Mazumder M, Ahmed R, WajahatAli A, Lee SJ. SEM and ESEM techniques used for analysis of asphalt binder and mixture: A state of the art review. *Constr Build Mater*. 2018. <https://doi.org/10.1016/j.conbuildmat.2018.07.126>.
47. Jalal FE, et al. On the recent trends in expansive soil stabilization using calcium-based stabilizer materials (CSMs): a comprehensive review. *Adv Mater Sci Eng*. 2020. <https://doi.org/10.1155/2020/1510969>.
48. Li Y, Wu S, Dai Y, Pang L, Liu Q, Xie J, Kong D. Investigation of sodium stearate organically modified LDHs effect on the anti-aging properties of asphalt binder. *Constr Build Mater*. 2018. <https://doi.org/10.1016/j.conbuildmat.2018.03.181>.
49. Ahmed A. Compressive strength and microstructure of soft clay soil stabilized with recycled basanite. *Appl Clay Sci*. 2015. <https://doi.org/10.1016/j.clay.2014.11.031>.
50. Nahar N, et al. Shear behavior of treated soil by rice husk ash and cement. *Agric Eng Int*. 2023;25(3):22–30.
51. Ramesh HN, Manjunatha BV. Justification of strength properties of microstructural changes in the black cotton soil stabilized with rice husk ash and carbide lime in the presence of sodium salts. *SN Applied Sciences*. 2020. <https://doi.org/10.1007/s42452-020-2226-1>.
52. Yang J, Ding Q, Zhang G, Hou D, Zhao M, Cao J. Effect of sulfate attack on the composition and micro-mechanical properties of CASH gel in cement-slag paste: A combined study of nanoindentation and SEM-EDS. *Constr Build Mater*. 2022. <https://doi.org/10.1016/j.conbuildmat.2022.128275>.
53. Pradhan SS, Mishra U, Biswal SK. Mechanical and microstructural study of slag based alkali activated concrete incorporating RHA. *Constr Build Mater*. 2023. <https://doi.org/10.1016/j.conbuildmat.2023.132685>.